Sandhiya and Ubaidulla
Bulletin of the National Research Centre (2022) 46:234
https://doi.org/10.1186/s42269-022-00909-7

Bulletin of the National Research Centre

RESEARCH

Open Access

Enhancing cellular uptake and membrane permeability of gallic acid for breast cancer therapy via folate-tagged PEGylated iron oxide nanoparticles has theronastic agent

V. Sandhiya* and U. Ubaidulla

Abstract

Background: In an attempt to prove biological activity enhancement upon escalating the cellular uptake response through ligand and carrier-based via nanoframework, gallic acid was chosen to be formulated into PLGA-based polymeric nanoparticles with iron oxide as the theranostic agent.

Results: The pre-formulation studies like FTIR, DSC, XRD, and TGA were carried out, which implies good compatibility between drug and polymer. Furthermore, the nanoparticles were prepared by using a single nanoprecipitation method, and the prepared nanoparticles were optimized using the Box–Behnken design. This design was used to optimize the gallic acid-loaded PEGylated nanoparticles by considering the effects of three factors (X_1; lipid, X_2; PLGA, and X_3; drug) on the response variables Y_1 (EE), Y_2 (size), and Y_3 (drug release). The findings of surface response plots are attributed to an optimized nanoparticle. The in vitro drug release followed a biphasic release profile in both tested media, pH 4.8 and 7.4. The desirable physicochemical characteristics involved small particle size with considerable stability, which was attained due to the anionic nature of PLGA. The in vitro cytotoxicity assay of gallic acid, GA/PLGA-IONPs, and optimized FA-GA/PLGA-PEGylated-LIONPs were evaluated using the MTT assay, which showed an inhibition effect on MCF-7 cells to induce apoptosis. Cellular uptake and fluorescence studies show higher cellular uptake and destruction of cells based on concentration dependence.

Conclusions: The above results show that prepared nanoparticles sustain the therapeutic concentration of the drug on target cells by enhancing permeability through the PEGylated lipid delivery system.

Keywords: Gallic acid/PLGA nanoparticle, Folate-tagged lipid nanoparticles, PEGylation, Cytotoxicity, Cellular uptake study, Breast cancer cells

Background

Nanotechnology is a branch of applied science and technology that deals with the development of devices and dosage forms. Nanotechnology has enormous application in the medical field to deliver drugs to target sites. With the help of vectors, nanoparticles are used to maintain the activity of the loaded drugs. Specifically, nanotechnology entities can be used to overcome problems such as half-life, low solubility, and toxicity, which will help to deliver conventional natural products more efficiently to the target site with the help of vectors. (Priyadarshani et al. 2021). It states that conjugates of nanosize can penetrate deeper into tumours, are efficiently endocytosed, and work against primary and metastatic tumours. Nowadays, phenolic compounds have more attraction towards cancer therapy due to their higher antioxidant properties, for example, gallic acid, ellagic

*Correspondence: sandhiyavaithi@gmail.com

Department of Pharmaceutics, C.L.Baid Metha College of Pharmacy, Thoraipakkam, Chennai 600097, India

acid, quercetin, rutin, ferulic acid, etc. Gallic acid is a polyphenolic compound found in plants and fruits. It is known to have anticancer, antimicrobial, etc. Research by Wang et al. (2014) showed that gallic acid has anticancer effects on MCF-7 cells by inhibiting cancer cell proliferation and inducing apoptosis. Nevertheless, the benefits of the phenols were found to be largely restricted due to multiple intrinsic properties such as the unpleasant oral taste, low water solubility, and poor intestinal bioavailability. Moreover, due to its hydrophilic nature, it is difficult to penetrate the cell membrane. Therefore, nanotechnology is one of the recently evidenced solutions that provides superior rewards to overcome these limitations (Attallah et al. 2020). To increase the efficacy, the drug has been loaded with PLGA polymers (Ali sartaj et al. 2021), which is one of the highly evidenced biopolymers in carrying and shielding a drug, targeting its delivery and controlling the release rate (Nouran et al. 2022) This could prevent dose dumping and keep the therapeutic on cancer cells (Hiren Kumar et al. 2011). Study aims to prepare gallic acid/PLGA nanoparticles with iron oxide. Here, iron oxide serves as a drug carrier for water-soluble drugs due to its higher hydrophobicity property. Previous studies reported that the magnetic properties of iron oxide nanoparticles have been developed for anticancer activity with functionalized drugs, but failed to report that due to small size and higher surface volume, the size of the nanoparticle will get aggregated and lead to the form of a higher size, which might directly affect the penetration rate. To overcome this, (Shah et al. 2017) suggested that gallic acid is exerted to control the size of the particle. The presence of a phenyl group increases steric hindrance, thereby preventing aggregation of IONPs through the formation of chelate as ferrous gallate and stabilizing the size of the particle. Shah et al. (2017) reported that surface opsonization of nanoparticles promotes the removal of nanoparticles from the circulation within sec to min through the MPS system. According to (Denadorniani et al. 2014), gallic acid-loaded IONPs coated with PEG have increased plasma retention time (Abuzer Alp et al. 2020; Su et al. 2016). That PEG in NPs often affects the encapsulation efficiency of loaded molecules and also alters their recognition ability for targeted delivery. As the mole fraction of PEG–lipid increases, the membrane's permeability increases, making the encapsulated drug escape unfavourable for drug delivery. The encapsulation efficiency of water-soluble drugs decreases with an increase in the PEG-containing lipid content. The possible reason is that PEG will occupy the volume of NPs, and the larger the molecular weight of PEG, the more the volume is taken. The method used to solve this problem is the introduction of PEG into the pre-formed NPs so that PEG is grafted on the surface of the NPs instead of in the core of it, reducing the volume of the body occupied by PEG. For hydrophobic drugs encapsulated in the micelle core by hydrophobic interaction, the maximum drug-loading capacity increases significantly with the increase in the molecular weight of PEG. The reason might be that the hydrophilic shell formed by long-chain PEG prevents drug desorption from the micelle core. According to (Angelo Nicosia et al. 2021; Ramasamy Bhanumathi et al. 2018), non-specific nanoparticles cause significant systemic toxicity. This can be overcome by the conjugation of PEG and functionalized folic acid through hydrogen bonding. (Farran et al. 2020) reported folate receptors have higher expression on tumour cells, rapid receptor recirculation after cell internalization, etc., moreover as targeting ligands, improved stability and increased stability in acidic or basic media, and better resistance to high temperatures. (Norton et al. 2020) reported that folic acid carries no risk of toxicity or immune reactions. Therefore, folate delivery systems can potentially maximize therapeutic efficacy while minimizing side effects (Agabeigi et al. 2020). Their results revealed an increase in apoptotic induction via reactive oxygen species and condensed nuclei in cancer cells.

Thus, this study proposes to assess the anti-tumour activity of gallic acid, gallic acid-loaded iron oxide nanoparticles, and folate-conjugated gallic acid-loaded PEGylated lipid iron oxide nanoparticles. In this study, gallic acid was encapsulated in PLGA to increase the efficacy. Interestingly, the PLGA and gallic acid core were coated with iron oxide to control the size and improve the drug delivery system. As gallic acid iron oxide nanoparticles, the size-control effect has been exerted by gallic acid through the presence of phenyl group, which provides sufficient steric force to minimize the aggregation of iron oxide nanoparticles (Ruben Correcher et al. 2021). A previous study suggested that the charge and hydrophobic and hydrophilic properties of the surface of nanoparticles influence their interaction with proteins and cell membranes. Therefore, the nanoparticles have been cleared off by the biological system through the RES system. However, because PEGylation coating can bind with plasma protein and most likely retain natural conformation, the recognition system fails to identify the underlying nanoparticles as foreign bodies, resulting in increased circulation time. Despite increasing the uptake by cancer cells, lipids are used as anchoring materials to enhance the permeability and retention effect through the caveolin-mediated endocytosis pathway (Saad Niaz et al. 2022). Due to the flexibility, the nanoparticles deform the surface membrane and lead to engulfment. In order to specific targeting and to reduce the side effects, folate has been used as

a surface conjugation moiety. Through the receptor-mediated process, it might target the cancer cells specifically and increase the cytotoxicity effect.

PLGA (poly-D, L-lactide-co-glycolide) and gallic acid were procured from Sigma-Aldrich. As a gift, iron oxide and ammonium hydroxide were obtained as a gift sample from MEDOPHARM Pvt.Ltd. L-phosphatidylcholine and DSPE-PEG2k-FA were procured from commercial companies. The MCF-7 (human breast adenocarcinoma) cell line was procured from NCCS (Research Institute in Pune). The list of chemicals needed for the cytotoxic assay was acquired from Greenmed lab, Thoraipakkam.

Methods

Preparation of FA-gallic acid/PLGA-PEGylated lipid IO nanoparticles

Gallic acid is dissolved in acetonitrile and added into the PLGA polymeric solution, and the mixture is stirred for 1 h until a clear solution is obtained. The mixture of ferrous chloride tetrahydrate ($FeCl_24H_2O$) and ferric chloride hexahydrate ($FeCl_36H_2O$) was then sonicated for 1 h separately with 6 ml of ammonium hydroxide. Then, the polymer and drug mixture were added into the above mixture to get the iron oxide core. This core formation was achieved by the interaction of gallic acid with ionic iron at the surface of the nanocore, which increases the reactivity and favours uniform dispersion. The mixture was also stirred for 24 h to produce iron oxide nanoparticles (Xiao Hu et al. 2016). Then, the nanoparticles were dipped in the pre-warmed L-phosphatidylcholine/DSPE-PEG4k-FA mixture and stirred slowly in a shaker for 3–5 h at room temperature. After completion, the solution was centrifuged to remove recalcitrant organic molecules, and the settled nanoparticles were washed and dried. Finally, the surface-modified nanoparticles were collected successfully.

Optimization method (Box–Behnken design)

Experimental design

Our preliminary experimental findings revealed that the design and evaluation of nanoparticles are influenced by three factors, namely the concentration of polymer, lipid, and drug. Response surface methodology using Box–Behnken design (Saba Ibrahim et al. 2021) was chosen because it allows determination of the influence of these factors on the nanoparticle properties with a minimum number of experiments. A Box–Behnken design was used to investigate the effects of three factors (X_1; polymer, X_2; lipid, and X_3; drug) on the response variables Y_1 (entrapment efficiency), Y_2 (particle size), and Y_3 (drug release).

Table 1 lists the independent factors and the dependent variables used in the design. The response surface of the variables inside the experimental domain was analysed using stat Ease design expert software (version no. 10, MacOS) (Ubaidulla 2008). The statistical design provides a polynomial describing the quadratic effect (Deepthi et al. 2017), as well as the interactions of each study factor on the considerable response variable. The general model corresponds to the following equation:

$$\begin{aligned} Y_0 = {} & b_0 + b_1A + b_2B + b_3C + b_{12}AB \\ & + b_{13}AC + b_{23}BC + b_{23}BC + b_{23}BC \\ & + b_{23}BC + b_{23}BC + b_{11}A_2 + b_{22}B_2 + b_{33}C_2 \end{aligned}$$

Y is the measured response associated with each factor–level combination; b_0 is an intercept; b_1–b_{23} are the regression coefficients; and X_1, X_2, and X_3 are the independent variables. The results are shown in Tables 1, 2, and 3 and Fig. 1.

The characterization of nanoparticles

FTIR study: Fourier-transform infrared spectra of the materials were performed over the range of 400–4000 cm^1 with 4 cm^1 resolution, using a KBR disc method with approximately 1% of the sample in 200 mg

Table 1 The formulation factors and responses of Box–Behnken design for gallic acid nanoparticle

Factor	Name	Units	Level used (Low − 1)	Level used (High + 1)
A:X_1	Lipid conc	% w/v	1	4
B:X_2	Polymer	% w/v	0.5	1
C:X_3	Drug	Mg	5	25
Response	**Name**	**Units**		**Goal**
Y_1	Particle size	Nm		Minimum
Y_2	Entrapment efficiency	%		maximum
Y_3	Drug release (48 h)	%		Maximum

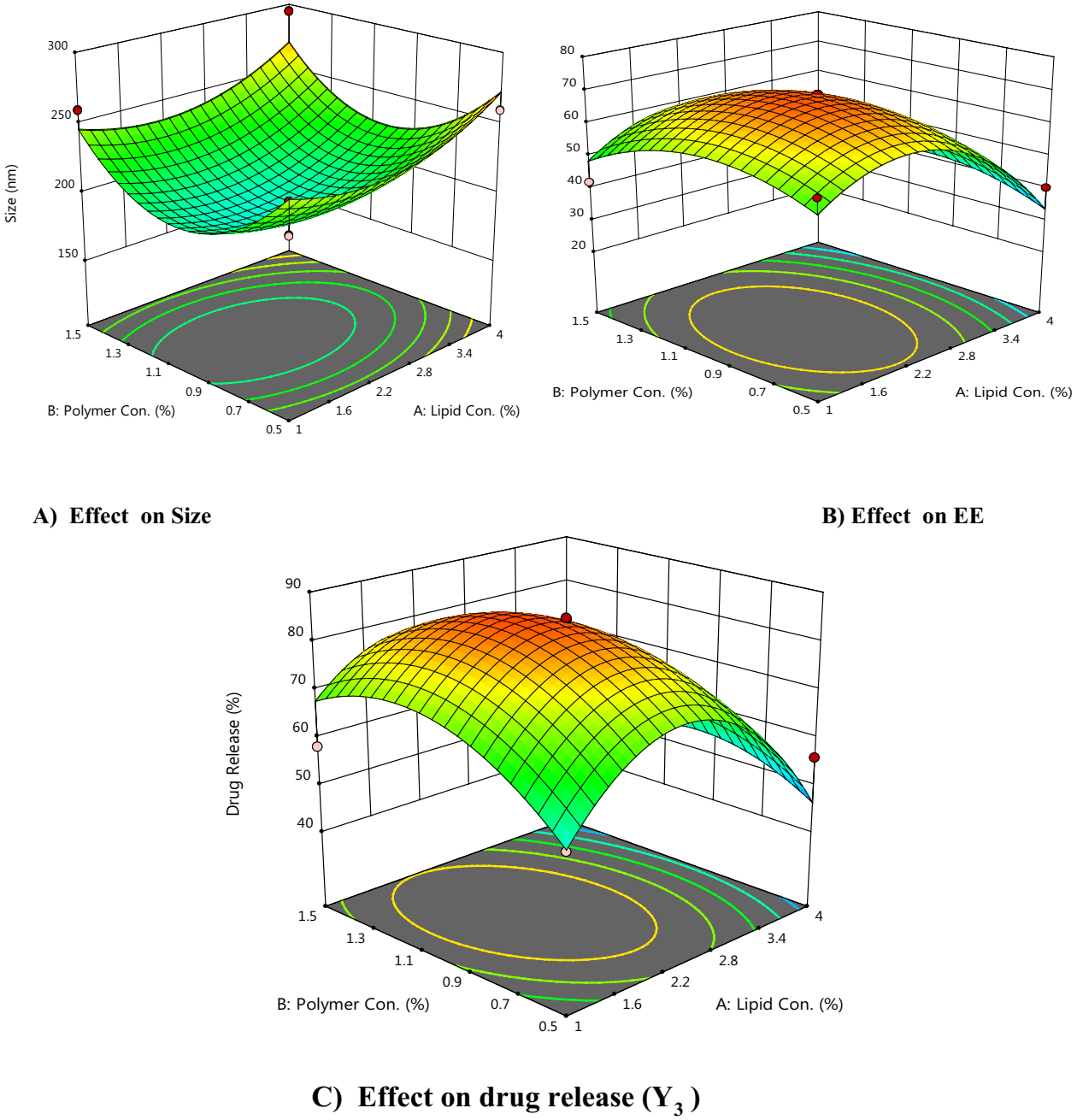

Fig. 1 Effect of responses by prepared GANPs

of spectroscopic grade potassium bromide, and the pellets were pressed at 10 tons. The outcomes are shown in Fig. 2.

XRD: The powders of samples were packed strongly in a rectangular aluminium cell, and the samples were exposed to the X-ray beam. The scanning region of the diffraction angle, 2, is 5–80. At room temperature, duplicate measurements were taken. The results are shown in Fig. 4.

Differential scanning calorimetry (DSC): The sample (approx. 2 mg) was sealed in a crimped aluminium cell and heated at a speed of 10 °C/min from 50 to 300 °C in an atmosphere of nitrogen. And finally, the data were recorded. The results are shown in Fig. 3.

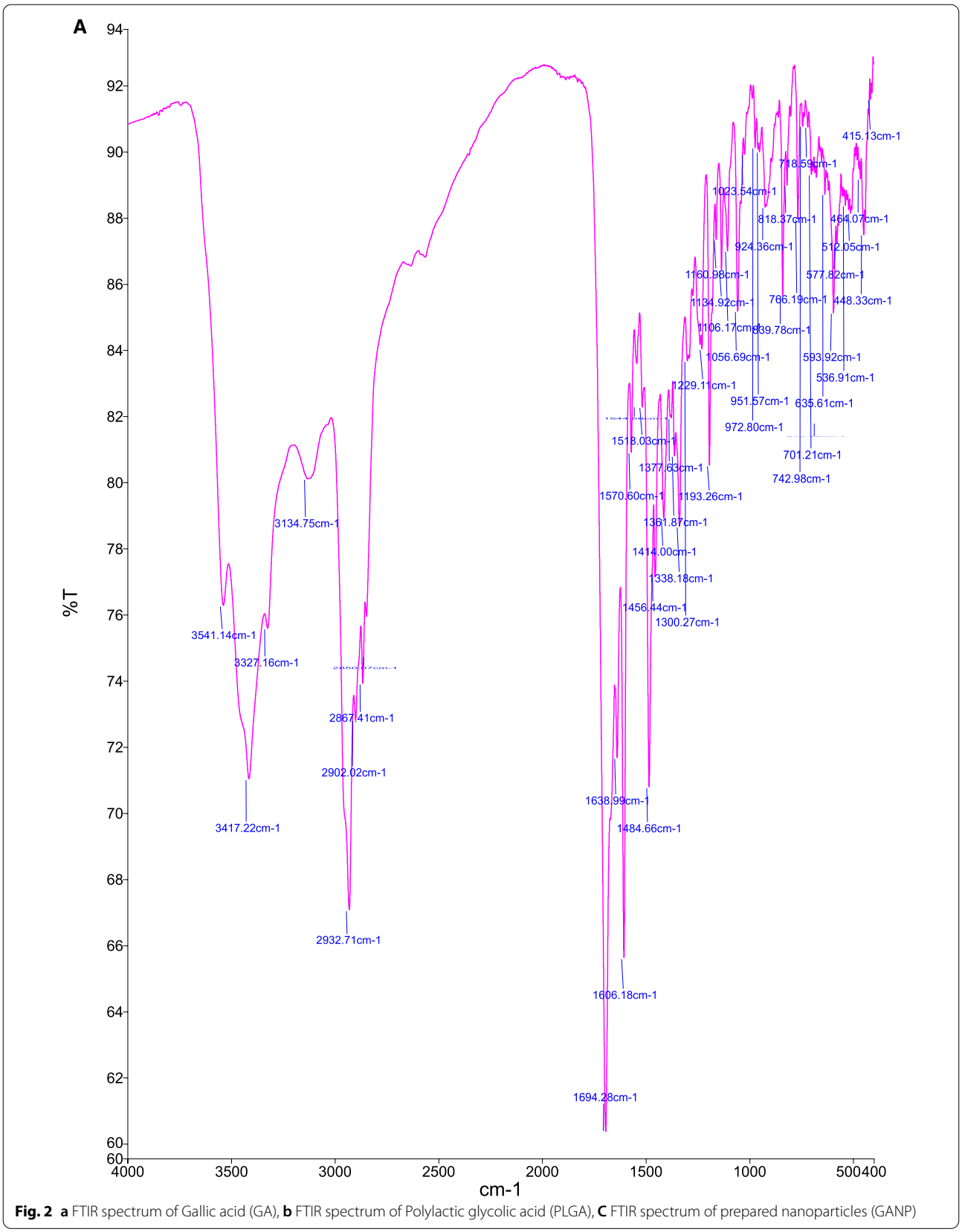

Fig. 2 **a** FTIR spectrum of Gallic acid (GA), **b** FTIR spectrum of Polylactic glycolic acid (PLGA), **C** FTIR spectrum of prepared nanoparticles (GANP)

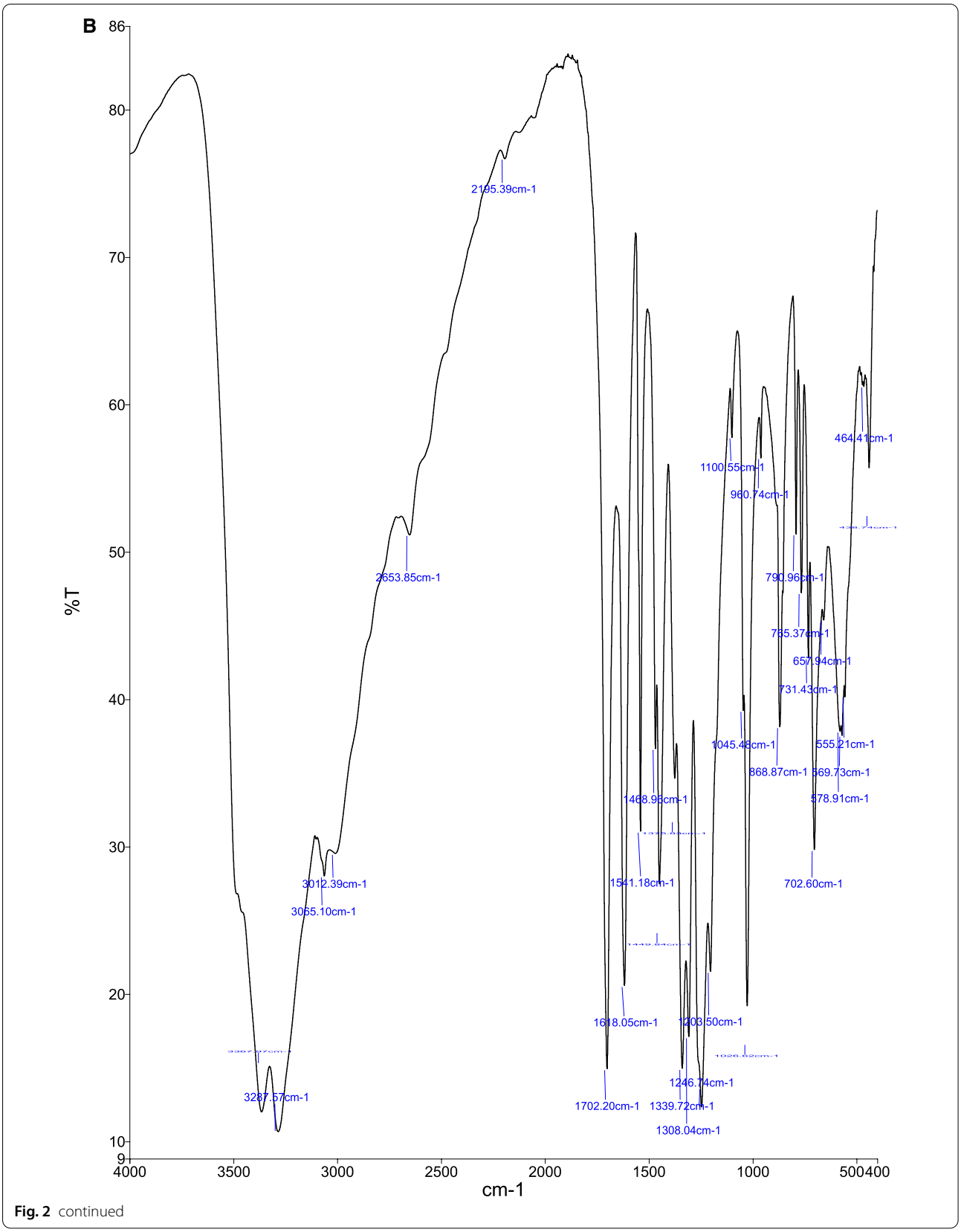

Fig. 2 continued

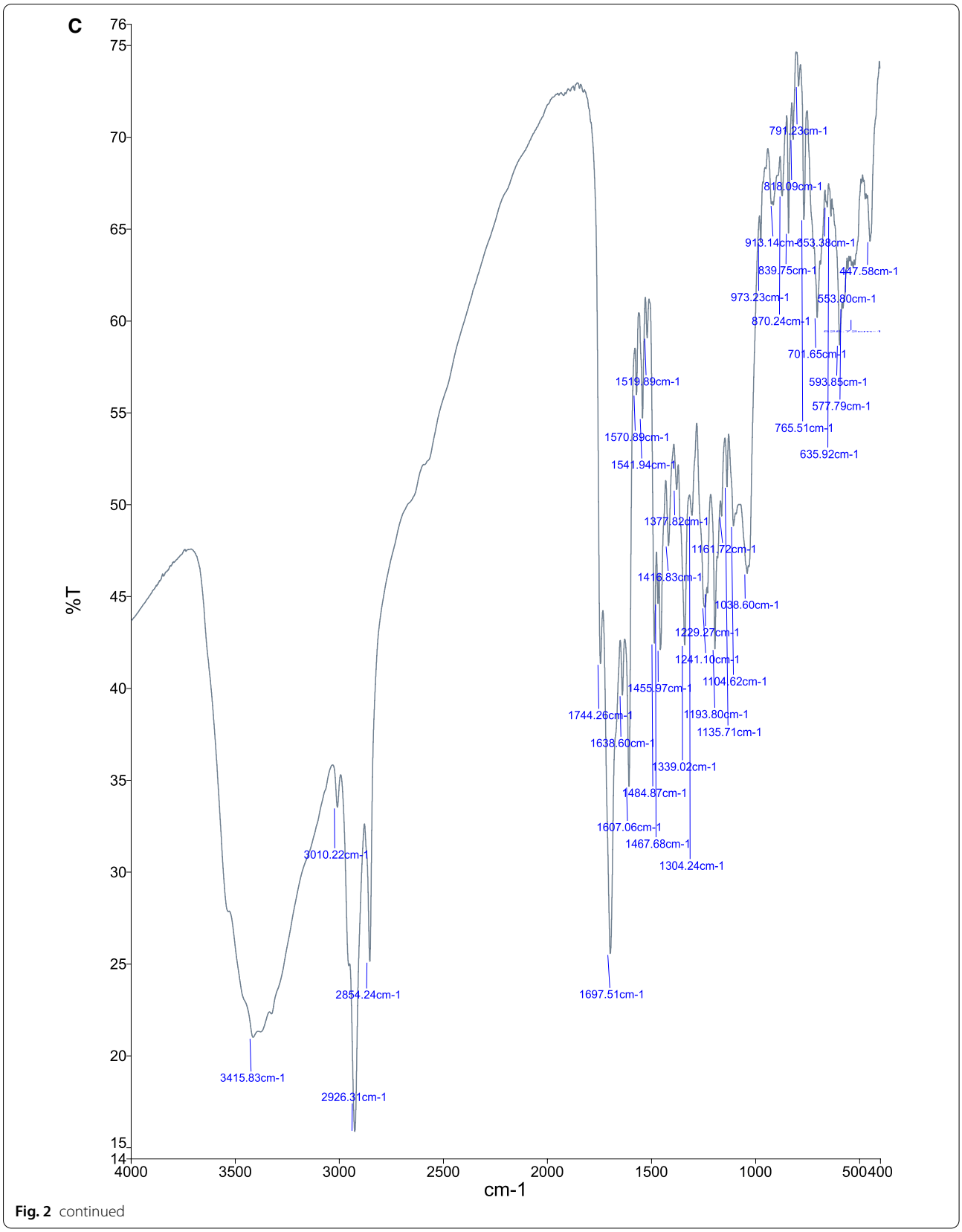

Fig. 2 continued

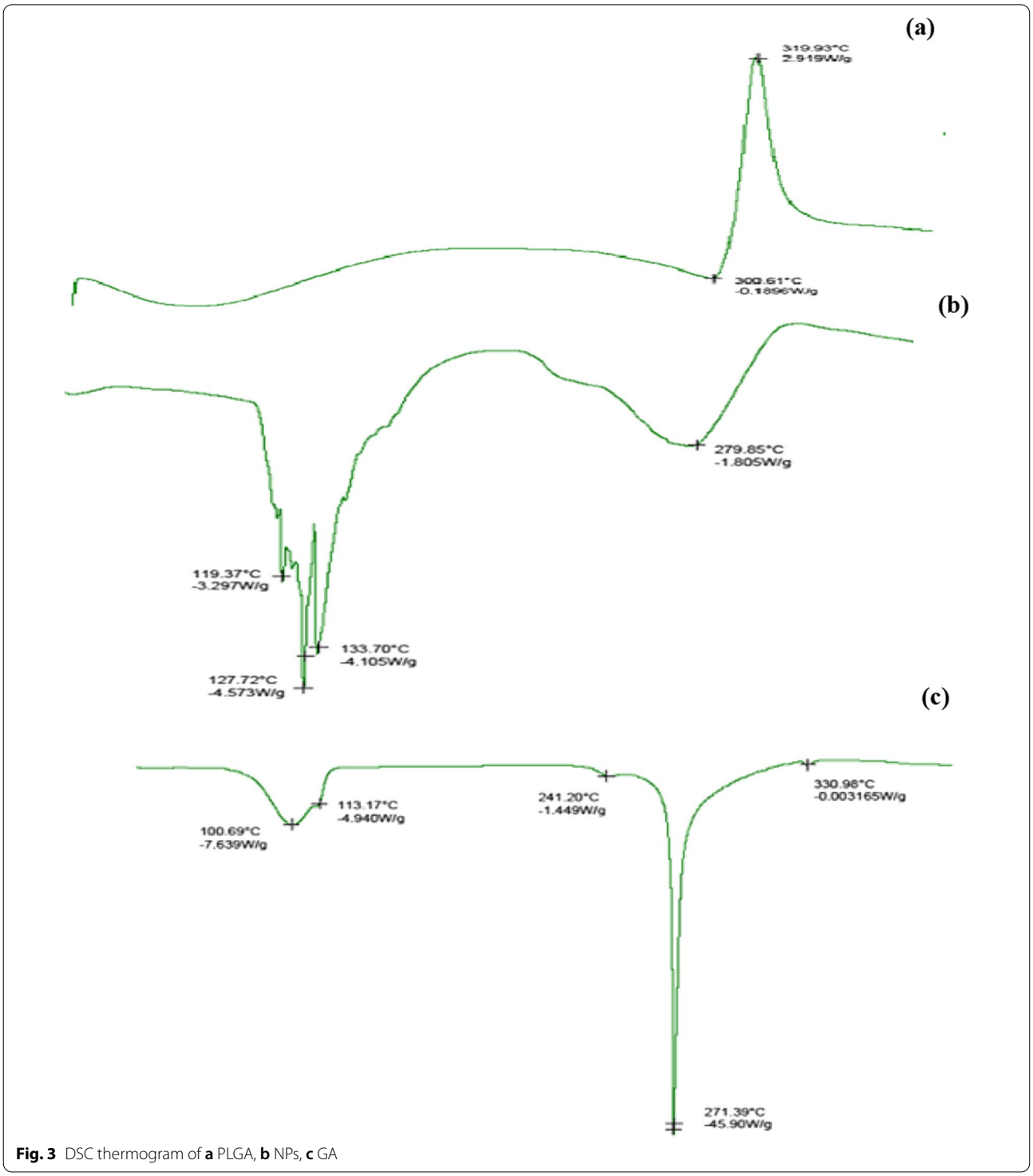

Fig. 3 DSC thermogram of **a** PLGA, **b** NPs, **c** GA

Entrapment efficiency: The prepared nanoparticles weighed 20 mg and were completely dissolved in 10 ml of DMSO. Then, the residue was washed and diluted by gently shaking for 24 h at 37 °C. Then, the solution was centrifuged at 16,000 g for 15 min, and the supernatant was collected. An aliquot of 1 ml of supernatant was diluted to 10 ml with DMSO, and adsorbance was measured in UV at 264 nm for gallic acid.

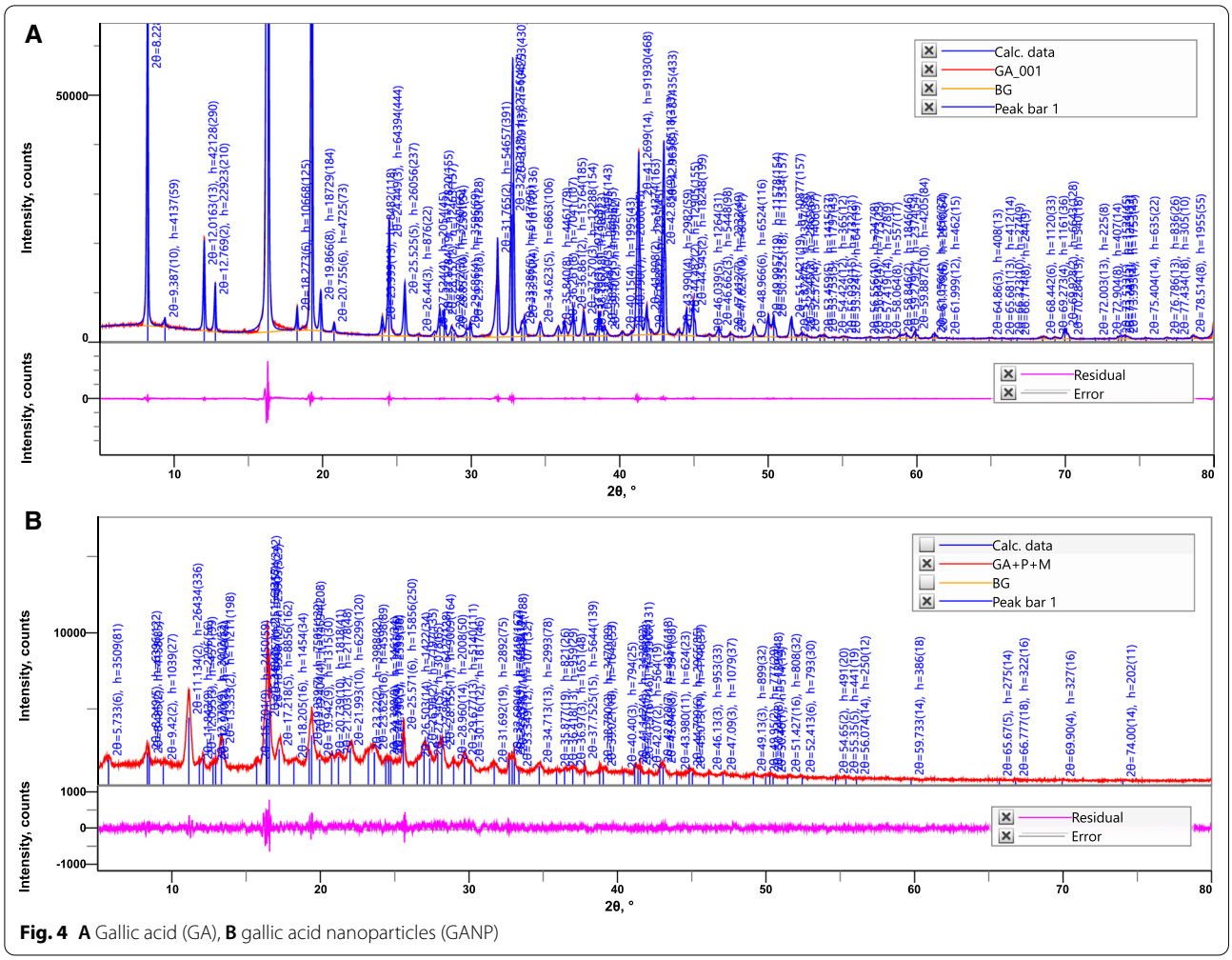

Fig. 4 **A** Gallic acid (GA), **B** gallic acid nanoparticles (GANP)

$$\%\, w/w \text{ drug loading content} = \frac{\text{weight of drug in nanoparticles}}{\text{The weight of removed nanoparticles}} \times 100$$

$$\text{Entrapment efficiency (\%) w/w} = \frac{\text{weight of drug in nanoparticles}}{\text{The initial weight of the drug fed}} \times 100$$

Scanning electron microscopy The sample was sprinkled on double-sided carbon tape and placed on a brass stub. The surface was coated with a thin layer of palladium (about 30 m) in an auto fine coater. Then, it was placed in the sample chamber of a scanning electron microscope and the morphology of the complex was observed. The results are shown in Fig. 7.

Transmission electron microscopy (TEM) 5 ml of the nanoparticle suspension was placed on a carbon form varcoated grid and left to adsorb for 2 min. After adsorption, the grid was washed with deionized water to remove the excess suspension. The grid was visualized by TEM using a microscope operated at 60 kV.

Surface zeta potential measurements were measured using the laser zeta meter The nanoparticle samples (2.5 ml) were diluted with double distilled water (50 ml) with NaCl as the suspending electrolyte solution. The pH was adjusted to the required value. The samples were shaken for 30 min. After shaking, the equilibrium pH was recorded and the zeta potential of the particles was

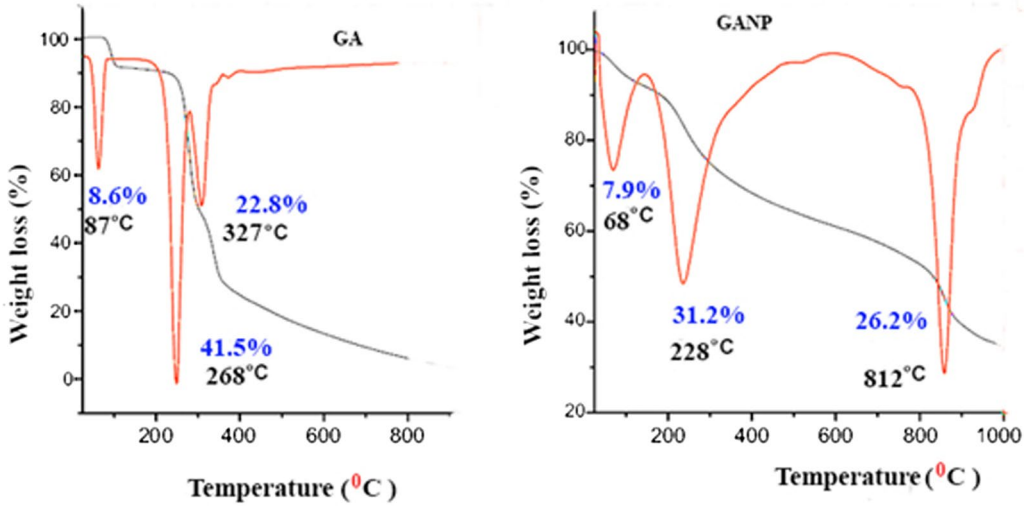

Fig. 5 TGA graph of GA and GANP

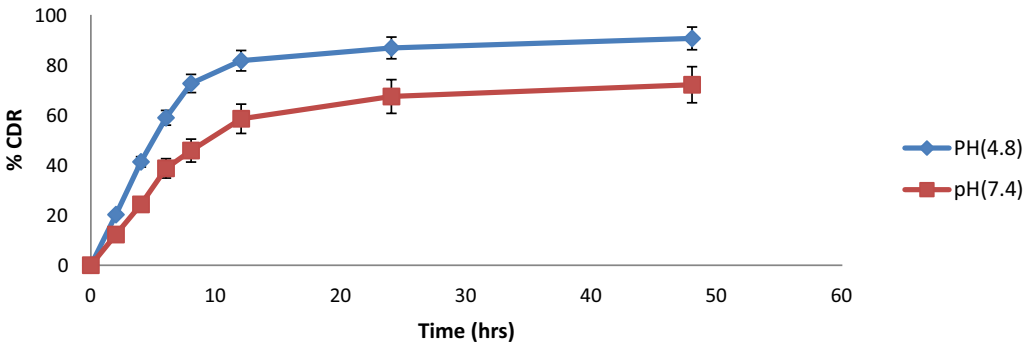

Fig. 6 Optimized formulation of gallic acid nanocomposite

measured. The results are revealed in Fig. 9. The analysis was carried out at a scattering angle of 90°A at a temperature of 25 °C using nanoparticles dispersed in deionized distilled water. (2 mg of sample was dissolved in 5 ml of deionized water, and then, sonication was done in a sonicator.)

TGA/DTG Thermogravimetry (TGA) and differential thermogravimetry (DTG) were performed in 150 L alumina crucibles using a Mettler-Toledo instrument at a heating rate of 10 degrees per minute in the range of 20–1000 °C. The results are shown in Fig. 5.

In vitro diffusion study of gallic acid nanoparticles An in vitro release study of GANPs was conducted in the Franz diffusion cell. The drug release profiles of gallic acid from nanoparticles were carried out at pH 7.4 and 4.8 (Sinha et al. 2018). A 5 mL aqueous dispersion of GA-PLGA-NPs was loaded into the cylinder and coupled to the diffusion cell containing the receptor phase. The dissolution medium was agitated at 25 rpm using a magnetic stirrer. At different time intervals, aliquots of 2 ml were withdrawn and immediately restored with the same volume of buffer solution pH 7.4 and 4.8. The amount of GA released was assessed by a double-beam UV spectrophotometer at 264 nm. The report is represented in Fig. 6.

Kinetic study

Data from in vitro dissolution experiments were analysed using kinetic equations such as zero-order, first-order, Higuchi model, Hixson–Crowell, and Korsmeyer–Peppas. The coefficient of correlation (r^2) and constant (k) values were calculated for the linear curves obtained by regression analysis of the plots. The release data obtained via the above procedure were subjected to the *R* and Peppas model to devise its

release mechanism. The percentage of drug release can be determined by the diffusion exponent equation. The equation is:

$$M_t/M = K_{tn}$$

where M_t is the amount of drug released at time t, M is the nominal total amount of drug released, K is the kinetic constant, and n is the diffusion exponent that is used to characterize the release mechanism. For nanoparticles, a value of n is 0.61, which is an indication of non-fiction release (both diffusion and controlled drug release).

Vibrating sample magnetometry study

10 mg of prepared iron oxide nanoparticles and FA-GA/PLGA-PEGylated-LIONPs were weighed and placed in a separate container, then wrapped with wax to maintain position, and placed in a sample holding rod and kept in between the magnetic field poles. Then, the vibration of the samples was amplified and recorded as a magnetic moment. The result is shown in Fig. 8.

In vitro cytotoxicity test

Gallic acid-loaded iron oxide nanoparticles, gallic acid-loaded iron oxide nanoparticles with PEG/lipid coating, gallic acid-loaded iron oxide with PEG/lipid coating, and FA were prepared and sterilized by membrane filtration before the MTT assay. The assay is used to determine the surviving cell numbers through MTT dye reduction. Here, the dye is reduced by live cells to purple formazan. MCF-7 cell lines were treated with samples, and plates were incubated at 37 °C in a 5% CO2 atmosphere for 24 h. After incubation, the test solutions in the wells were discarded, and 100 l of MTT (5 mg/10 ml of MTT in PBS) was added to each well. The plates were incubated for 4 h at 37 °C in a 5% CO_2 atmosphere. The supernatant was removed, 100 l of DMSO was added, and the plate was gently shaken to solubilize the formed formazan. The absorbance was measured using the following formula: The result is shown in Fig. 10.

$$\text{Cell viability (\%)} = \left(\text{OD Sample (optical density)} - \text{OD blank}\right) \times 100$$

Study of cellular internalization

Each confocal dish was seeded with 1×10^5 MCF-7 cells (20 mm in diameter, glass-bottom). For cell adhesion, cells were cultured for an entire night. Following a 4-h incubation with FITC at concentrations of 5 g/mL, 10 g/mL, 20 g/mL, and 40 g/mL, the cells were fixed and permeabilized with 3.8 per cent paraformaldehyde and 0.1 per cent Triton X-100, respectively. With DAPI, the cell nucleus was stained. Cells were examined using DAPI, Rhodamine, and FITC filters under the Olympus FV3000 microscope after being washed with PBS. As a control, cells were treated with FITC of same concentration. The outcome is displayed in Fig. 11.

Fluorescent labelling for research of nuclear morphology

MCF-7 cells were seeded onto a coverslip of a 24-well flat-bottom microplate (1×10^5 cells/well density) and cultured for the night at 37 °C in a CO_2 incubator. They were given the IC50 dose of FA-conjugated GA/PLGA-PEGylated LIONPs and then incubated for 48 h at 37 °C. The cells were then fixed with a 4 per cent paraformaldehyde solution for 30 min after being rinsed twice with PBS. After 5 min of dark, room-temperature DAPI incubation on fixed cells, the cells were washed twice with PBS and studied under a fluorescence microscope. In representative fields, the quantity of apoptotic cells was counted, and the percentage of apoptotic cells was calculated. The results are shown in Fig. 12.

Results

Discussion

Optimization of formulation factors of gallic acid-loaded PLGA nanoparticles is represented in Table 1, and the study was designed to determine the effects of three factors: (A; X_1) lipid concentration, (B; X_2) PLGA polymer concentration, and (C; X_3) gallic acid concentration. The results of Y_1 (entrapment efficiency), Y_2 (size), and Y_3 (drug release) are represented in Table 2. The preparation of gallic acid-loaded PLGA nanoparticles was performed using a single-step emulsification method (Ade Arsianti et al. 2020).

Effect of the independent variables on the particle size (Y_1)

The aim of the study is to minimize the particle size. The results are displayed in Fig. 1. Here, the concentration of polymers plays a significant role in the size of the nanoparticles along with drug release from the matrix. The average particle size of the prepared nanoparticles was found to be in the range of 154.2 nm.

The effect on particle size can be explained by the following quadratic equation:

$$\begin{aligned} Y_1 &= 154.2 + 1.1804X_1 + 6.453X_2 - 0.976X_3 \\ &\quad + 10.786\,X_1\,X_2 - 0.268X_1\,X_3 + 16.843X_2\,X_3 \\ &\quad + 2.894X_{12} + 12.806X_{22} - 0.859X_{32}\,Y_2 \\ &= 154.2 + 1.1804X_1 + 6.453X_2 - 0.976X_3 \\ &\quad + 10.786\,X_1\,X_2 - 0.268X_1\,X \end{aligned}$$

A positive sign represented a synergistic effect, while a negative sign represented an antagonistic effect. The model was found to be significant (F-value = 24.74; $P < 0.001$). The values for predicted (0.9654) and adjusted

(0.9496) square values were in reasonable agreement. The signal-to-noise ratio was found to be satisfactory, so this model could navigate the design space.

From the equation, it is clear that factor X_2 (PLGA) affected the particle size of the prepared nanoparticles. The increase in the concentration of X_1 factor increased the particle size drastically. The probable reason for an increase in particle size could be that during the emulsification process, an increase in polymer concentration led to an increase in the viscosity of the organic phase, which led to the formation of nanodroplets with a larger size at the interface at the stirring intensity. Herein, increased particle size has less surface area, which shows a negative response in drug entrapment.

On the other hand, factor X_1 shows a positive value, that is lipid. As the concentration of lipid increases, it significantly increases the particle size. This could probably be due to the solidification property of lecithin. According to the regression equation, particle size was directly affected by lipid ratio. It has a significant role in particle size. This response might be due to lipid with polymer resulting in the desired structure and shape. In contrast, a further increase in lipid concentration increases the accumulation of lipid content and hence the particle size. Moreover, from the previous studies, it was observed that nanoparticles less than 200 nm are efficient at passing the membrane and releasing the drug into the cytoplasm. So it was clear from the plot that the interaction of X_1 and X_2 synergistically affects the particle size.

Factor X_3, and drug concentration, showed a slight positive value compared to X_1 and X_2 factors. Figure 1A shows that particle size is directly proportional to drug concentration, with concentration increasing as polymer concentration increases. Frequency of collisions between particles during emulsification results in the fusion of semiformed particles, producing a collective increase in particle size. But increasing the concentration of the drug alone does not have much of a significant effect on the particle size of the prepared nanoparticles.

Effect on entrapment efficiency

Polynomial equation

$$\begin{aligned} Y_2 = {} & 74.2 + 1.984X_1 + 9.153X_2 + 0.976X_3 \\ & + 16.946\,X_1\,X_2 - 0.478X_1\,X_3 \\ & + 12.923X_2\,X_3 + 1.894X_{12} + 14.609X_{22} \\ & - 0.959X_{32}\,X_3 + 12.923X_2\,X_3 + 1.894X_{12} \\ & + 14.609X_{22} - 0.959X_{32} \end{aligned}$$

The model was found to be significant (F-value = 24.9; $P < 0.0001$). The values for predicted (0.9259) and adjusted (0.9416) R-squared values were reasonable in agreement. The signal-to-noise ratio was found to be satisfactory, so this model could navigate the design space.

Analysing the polynomial equation, it was found that the percentage of drug entrapment increases with an increase in X_1 factor concentration, and X_3 factor concentration. The increased state of viscosity of the organic phase due to an increase in factor X_2, polymer concentration, could increase resistance to drug diffusion into the medium, leading to the incorporation of more drugs into the nanoparticles. Increasing the content of the drug was found to be entrapped in nanoparticles with increased size. This may be due to an increase in the length of the diffusion pathway, which decreased the drug loss and resulted in maximum entrapment efficiency.

As revealed by factor X_1, lipid concentration had a significant effect on entrapment efficiency as revealed by the positive value in the quadratic equation. The results suggested that the EE increased rapidly as the lipid concentration increased probably due to the presence of triglycerides in lipids, which provide more space to accommodate excessive drugs as a core material. However, increasing the concentration of lipid from a regular crystal lattice under low temperature, which had an exclusive effect on entrapment, further increases in lipid ratio, might get saturated, promoting the expulsion of already entrapped drug from the solid matrix, which led to a decrease in the entrapment efficiency.

Factor X_3, drug concentration; an increase in the concentration of drug may enhance the entrapment efficiency. This could be based on the size of the nanoparticles, as the increased size of NPs has more space for the drug to be entrapped up to certain points. After that, the increase in particle size decreases the entrapment efficiency due to the saturation process, so further there will be no space for the drug to get entrapped inside the NPs. The remaining excess drugs tend to accumulate over the external surface of nanoparticles and give burst release when in contact with the medium. Furthermore, lipid and polymer restructurement plays an important role in the effect of drug release.

Effect on drug release

The model was found to be significant (F-value = 24.2; $P < 0.0001$). The values for predicted (0.9179) and adjusted (0.9286) R-squared values were in reasonable agreement. The signal-to-noise ratio was found to be satisfactory, so this model could navigate the design space.

Here, if the concentration of factor X_2, polymer, and factor X_3 drug concentration increases, there will be an increase in drug entrapment. Being soluble in the organic phase shows higher polymer interaction and gets maximum entrapment inside the polymer matrix. When coming in contact with the dispersing medium, the polymer

undergoes restructuration and provokes burst drug release. Here, increases in the concentration of factors X_2 and X_1 had a significant effect on drug entrapment and drug release. But if X_2 and X_1 increase with a decreased concentration of X_3, there will be an increase in the particle size with less entrapment due to less surface area. This may directly affect the release pattern of the drug in the dispersed medium. To promote the optimized release, the concentration of X_1, X_2, and X_3 should be in the moderate range. At the same time, X_1 and X_3 have a negative impact on drug release due to their concentration level. An increase in X_1 and a decrease in X_3 may increase particle size with less entrapment, so it can delay the drug release. At the same time, the therapeutic index of the drug will reach a minimum range. To achieve maximum drug release, the independent factors must be in the optimal ratio. Further increasing factor X_2 and X_1 concentration with optimized X_3 concentration may increase entrapment efficiency and increase the drug release too.

Optimization of formulation factors

After statistical analysis and assessment of the impact of individual factors on the response, the optimization of the prepared formulations was done by design expert software. Table 4, optimization, gives precise formulation parameters to achieve the desired goals of the selected responses.

Selected process factors with desirability (1.000).

As per the desirability, the goal of the optimization study is to minimize particle size, maximize entrapment efficiency, and maximize drug release. The optimum levels of formulation factors for an optimized formulation based on the Box–Behnken design were 1.5% w/v of PLGA polymer, 2.5% w/v of lipid, and 1% w/v of gallic acid nanoparticles, with predicted values of 154.4 ± 0.4 nm for particle size, 75.4 ± 0.3% of EE, and 90.4% of drug release (48 h). The optimized formulation was prepared using a single-solvent emulsification method, and the actual values of the responses were 157.80.6 nm for particle size, 76.8 ± 2% for EE, and 91.64% for drug release. The real values of responses were established to be close to the predicted values, which indicated the validity of the Box–Behnken design.

Statistical analysis based on ANOVA for the response surface quadratic model is presented in Table 4. The *P*-value for the model is less than 0.001, which indicates that it is a significant and desirable model. The large model *F*-value might occur due to noise in the experiments. The lack of fit of the *F*-value implies that lack of fit is not significant relative to pure error.

The model *F*-value implies the model is significant. There is only a 0.01% chance that an *F*-value of this large might occur due to noise. The *P*-values were less than 0.0001 and indicate model terms are significant. Values greater than 0.1000 indicate the model conditions are not significant. The lack of a *F*-value of 1.16 implies that the lack of fit is not significant relative to the pure error. A minor lack of fit is acceptable to fit with the model.

FTIR study

The FTIR spectrum of gallic acid, PLGA, and gallic acid nanoparticles is represented in Fig. 2. The IR spectrum of GA showed characteristic peaks at 3287 cm^{-1} (O–H stretching), indicating the presence of carboxylic acid, 3065.10 cm^{-1}, 3012.39 cm (alcohol/phenol O–H stretch), 1203.50 cm-11045.48 cm^{-1} (C–OH Stretch), 1541.18 cm^{-1}, 1618.05 cm^{-1}, and 1702.20 cm^{-1} (aromatic C–H bending, aromatic C=C bending) (Vishal 2012). The IR spectrum of PLGA showed characteristic peaks at 3468.73 cm^{-1} (N–H stretching), 1631.54 cm^{-1} (C=C stretching), and 1420.35 cm^{-1} (CH–OH), and the presence of alcohol (Wan Fatihah 2018). The result is shown in Fig. 2a, b.

The FTIR spectrum of the GA nanocomposite shows the characteristic peaks of GA, which confirms the drug loaded on the surface of PLGA. To ensure the presence of DSPE-PEG-FA, a strong band was absorbed at 1694 cm^{-1} and 1608 cm^{-1}, respectively, indicating the presence of the C=O and N–H (amine) groups, which are the most prominent groups present in the nanocomposite. The presence of a lipid molecule (phosphatidylcholine) in nanocomposites is confirmed by the hydroxyl stretching frequency at 3415 cm^{-1}, the C–H stretching band of a long fatty acid chain at 2926 cm^{-1} and 2854 cm^{-1}, P=O stretching at 1241, P–O–C stretching at 1104, and N (CH3)3 stretching at 973. (Abdelkader Hassani 2020) reported that the spectral band at 557 cm^{-1} indicates the presence of an iron oxide crystal lattice in the nanoparticles. However, the FA-GA/PLGA-PEGylated LIONPs spectrum showed the appearance of a new peak at 2456 cm^{-1} and a shift in the trans out-of-plane bend of the lipid from 980 to 966 cm^{-1}. The appearance of the new peaks and the shift in the peaks indicate the hydrophobic interactions between the lipophilic art of the folic acid and the lipophilic tail of the lecithin, as well as the electrostatic attraction between the negatively charged hydroxyl group of the gallic acid and the cationic surface charge of the NPs.

DSC study

The DSC thermogram of gallic acid, PLGA, and nanoparticles is shown in Fig. 3. The drug gallic acid shows two endothermic peaks: the first peak at 100.69 °C and 113.17 °C, suggesting the presence of water molecules, and the second thermogram with a sharp peak,

showing melting endotherms at 271.39 °C (Fig. 3c). The mild endothermic peaks at 241.20 °C might be the initial decomposition stage of gallic acid, and the peak at 330.98 °C might be the saturated stage of gallic acid. So, the melting point of gallic acid will increase from 241 to 271 °C (Radwan et al. 2020). Respectively, Fig. 3a shows the thermogram of pure PLGA. Here, no distinct melting point was observed because PLGA is amorphous in nature (Dorniani et al. 2016). The characteristic peak at 319.93 °C was related to the thermal decomposition of the polymer. The similar melting transition properties of PLGA-loaded nanoparticles remained unaffected during encapsulation. According to Ruchi Singh et al. (2020), the DSC thermogram of lecithin revealed a mild endothermic peak at 153 °C and another broad peak at 240 °C. The first peak indicates hot movements of the phospholipid polar chains, whereas the other peak indicates their transition from the gel form to the lipid crystal state. PEG and FA have mild and moderate endothermic peaks, which have been discussed in brief by Ruchi Singh et al. (2020). As the sharp peak of gallic acid vanished, the DSC analysis revealed no crystalline drug material in the FA-GA/PLGA-PEGylated LIONPs formulation (Fig. 3b). The absence of an endothermic peak of gallic acid in the thermogram of nanoparticles indicates that the drug might be entrapped in the PLGA matrix. Thus, the drug incorporated into the nanoparticles was in an amorphous or disordered-crystalline phase of molecular dispersion or solid solution state within the polymer matrix. However, the strong and prominent peaks of nanoparticles could be owed to the reorganization of the components in the nanoparticle system in a state different from their original molecular structures and the possible formation of a strong complex. Such complexation could have been facilitated via the hydrophobic attractions, hydrogen bonds, and electrostatic interactions between the various components of the prepared nanoparticles.

XRD study

The crystalline state of pure gallic acid is indicated by the sharp, intense peaks at 2 = 16.22°, 25.36°, and 27.64° (Fig. 4). (Wenjia Guo 2015) reported that the drug gallic acid has numerous sharp peaks other than these intense peaks, whose positions correspond to the periodic spacing of atoms. But these sharp peaks are predominantly seen in pure drugs like gallic acid, which has been observed in our results. The polymer PLGA lacked intense peaks at 2θ from 10° and 30°, displaying a dome-shaped region due to the amorphous state. The XRD reflection shows pure magnetite nanoparticles with a cubic inverse structure. Further, the diffraction peak appeared at the 2 θ values of 25°, 30°, 47°, and 63°, which corresponds to the presence of a lattice plane (Fig. 4). The peaks at 21.04° and 27.11° were responsible for the presence of the PEG moiety, and other diffraction peaks observed at 8.02° and 16.33° were due to the presence of folic acid in the nanoparticles (Dena Dorninni 2012). The diffraction peak appeared at 2 θ from 18.2° due to the presence of phosphatidylcholine (lecithin) as a coating layer of the nanoparticle. Owing to observing these characteristic peaks in the nanoparticles, it is evident that the coating process did not result in a phase change of the nanoparticles.

TGA study

TGA analysis is used to determine the thermal stability and physicochemical nature of a compound by % weight loss. Under atmospheric conditions, the TGA study of gallic acid, PLGA, and nanoparticles was analysed. The TGA analysis curve for gallic acid shows the first stage of weight loss at 87 °C (8.6%) (Baiti et al. 2015), which might have occurred because of the removal of crystalline water. The sharp TGA curves of gallic acid indicate the onset of weight loss at 268 °C (41.5%)) and (22.8%) at 327 °C. Figure 5 represents the curve thermogravimetric thermograms due to the coating of iron oxide. The first weight loss at 68 °C (7.9%) corresponded to the removal of free and chemically adsorbed water. The onset of degradation of iron oxide and dihydroxylation of gallic acid occurred at 227 °C, which is higher than the decomposition of pure gallic acid. The slow mass reduction at 812 °C (26.2%) is due to PLGA decomposition. The range of weight loss is higher than plain drug, so these observations indicate the presence of gallic acid in the nanoparticles.

In vitro release

The release profile of gallic acid is depicted in Fig. 6, where the gallic acid nanoparticles released a burst of gallic acid with a remarkably higher percentage of 40% at pH4.8 and 27% at pH7.4 after 4 h (Fig. 6). This release pattern may be attributed to the weak bond between PLGA and gallic acid in acidic pH, which might also be associated with drug desorbed upon contact with the dissolution medium, which is more prone to faster diffusion (Chunhua Yang 2020). These features might offer a therapeutic privilege to cancer cells by escalating the release of gallic acid. Cancer cells are continuously exposed to rapid shifts in the acid–base balance due to the limited blood supply, exposing them more to acidic pH. From previous studies, it has been observed that the biphasic pattern of drug releases might be due to the diminution content of the drug in the polymer matrix. Hence, there was a plateau stage that lasted for 48 h at pH 4.8 and 7.4. Furthermore, (Hassani 2020) believed that the higher emulsification property of lipid and the restructurability of

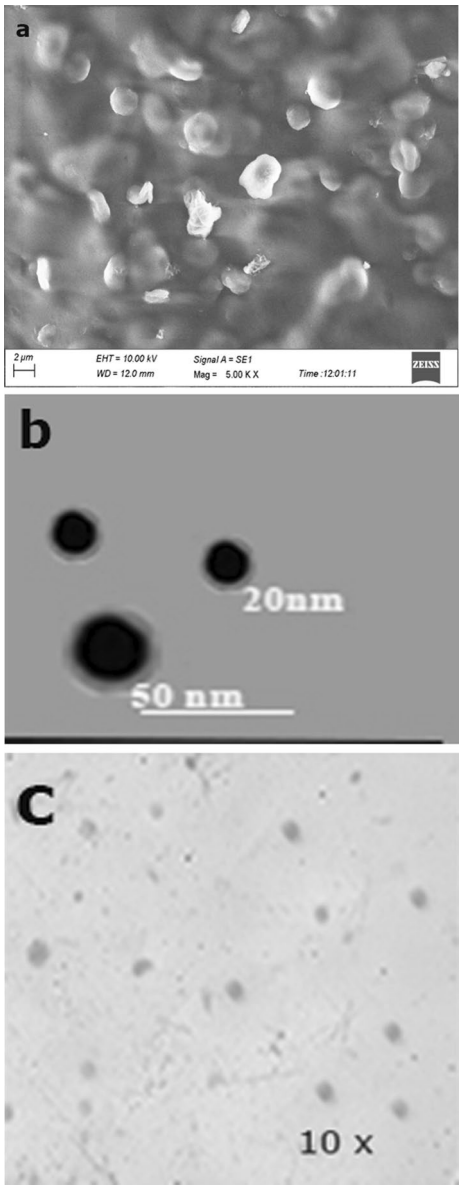

Fig. 7 **a** SEM, **b** TEM, **c** Optical microscopic images of optimized formulation

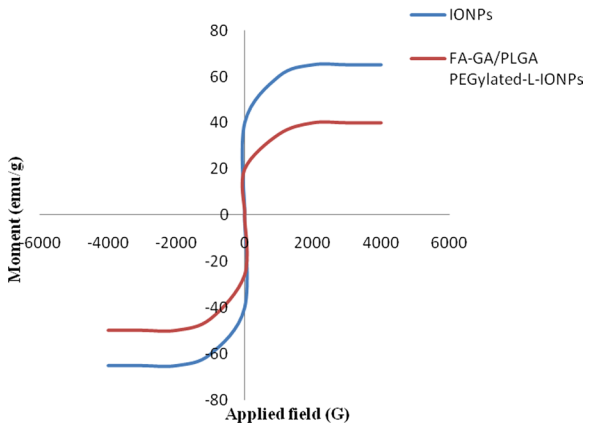

Fig. 8 Magnetic property study of IONPs, FA-GA PEG-LIPID-IONPs

PLGA could provide a higher affinity of drug exchange as an encapsulated agent. At pH 74, the solubility decreased with an increase in particle binding properties due to the stabilization of PLGA. These findings reveal that the polymer PLGA tended to disturb the release of drugs from nanoparticles at different pH.

Kinetic study

This study involves in vitro drug release using zero-order, first-order, Higuchi, and Korsmeyer–Peppas models. The graph for the Korsmeyer–Peppas model was plotted between log time and log percentage of drug remaining, and the correlation coefficient was found to be 0.947 for in vitro drug release, that is, almost unity for gallic acid NP and release exponent value (n) of 0.61; therefore, the best fit model for nanoparticles was the Korsmeyer–Peppas model. The release exponent value (n) was above 0.5, which suggests gallic acid release from nanoparticles followed non-Fickian diffusion.

SEM, TEM

SEM images revealed the prepared nanoparticles are spherical in shape, which might be attributed to the formation of iron cations chelate with gallic acid, which can lead to the formation of black ferrous or ferric gallate (Fig. 7a). (Basharat Khan 2021) reported that the presence of the phenyl group in gallic acid provides sufficient steric hindrance to minimize the agglomeration of nanoparticles. Moreover, the presence of a hydrophilic functional group could serve as a potential H-bonding site for iron oxide. These can remarkably lead to the form of a stable nanoparticle. In addition, the shape of NPs plays a pivotal role in the uptake mechanism. Herein, (Chithrani et al. 2006) revealed that the spherical shape of NPs had higher uptake compared to the rod shape of NPs. Further, the presence of a lipid coating over the nanoparticles was conceded by TEM analysis. Figure 7b represents the presence of a bilayer membrane over the dark spherical nanoparticles against a light background. TEM images would give a better understanding of the real geometric size of the particle, and the correlation between process variables and particle size would be seen on a qualitative basis as well (Fig. 7c). The optical microscopic images reveal the prepared formulation was nano in size, which was confirmed visually under a microscope. From the previous studies, it was observed that prepared nanoparticles are spherical and may enhance the cellular uptake facilities.

VSM

Gallic acid-loaded nanoparticles (Socoliuc et al. 2020) in Fig. 8 show hysteresis loops with saturation magnetization (M_s), remnant magnetization (M_r), and coercivity (H_c) parameters. The saturation magnetization of iron oxide nanoparticles was about 60.481 emu/g, the value of magnetization at the applied magnetic field (Mona Ebadi et al. 2021) enhanced with the increases in crystallinity. The folate-conjugated gallic acid-loaded PEGylated lipid iron oxide nanoparticles show 41.081 emu/g in Fig. 8. (Deepak Sharma et al. 2014) reported the decrease in saturation magnetization has been notified, and this could be the existence of coating materials over the nanoparticle. The findings reveal the nanoparticles have superparamagnetic performance. This might be responsible for the hyperthermia behaviour of iron oxide. According to the VSM results, the nanoparticles showed supermagnetic behaviour.

Zeta potential

The zeta potential provides information about the stability of the suspension. High values showed that there would be strong repellent forces between particles. The zeta potential value of prepared nanoparticles has a negative charge due to the dissociation of the negative charge generating groups like carboxylic groups of PLGA polymer (Brandenberger et al. 2010). Since most cellular membranes are negatively charged, zeta potential can affect nanoparticles' tendency to permeate membranes, with cationic particles generally displaying more toxicity associated with cell wall disruption (Fig. 9). In addition, the surface charge of nanoparticles affects the uptake mechanism of nanoparticles (Dausend et al. 2008). Here, more specifically, the internalization of negatively charged nanoparticles leads to gelation of the membrane and is mediated through the endocytosis pathway.

A remarkable size-control effect was exerted by GA on functionalized IONP. This might be due to a decrease in the magnetic dipole–dipole interaction among the aggregates during the formation of nanoparticles (Panariti et al. 2012). This could be attributed to strong coordination between bonding sites of gallic acid with iron oxide (Fig. 9). In the present study, the particle size of the nanoparticles depended on the concentration of lipid. As the concentration increases, the particle size also increases (Rejman et al. 2004). Our findings revealed the size of the prepared nanoparticles was found to be 154.4 nm. Moreover, from the previous studies, it was found that the proposed size of the nanoparticle is recommended for the invagination process of cancer cells through the clathrin- or caveolin-mediated endocytosis pathway (Ladan Rashidi 2014).

In vitro cell line study

The in vitro cytotoxicity study of gallic acid on cancer cells was analysed using an MTT assay. The result is shown in Fig. 10a, b.

The MTT assay of gallic acid-loaded PLGA nanoparticles showed their anticancer properties against MCF-7 cells and A54-9 cells, due to the reduction in cell viability, which was increased by the increase in gallic acid availability in the medium culture. The drug gallic acid showed 70% of cell viability at 100 µg/ml concentration, gallic acid-loaded iron oxide nanoparticles showed 38.8% of viability, and gallic acid-loaded iron oxide lipid nanoparticles showed 18% of viability at 100 µg/ml concentration in MCF-7 cells and showed 12% of viability at 100 µg/ml concentration in A54-9 cells. From the findings, it was observed that compared to pure gallic acid and gallic acid-loaded iron oxide nanoparticles, gallic acid-loaded PEGylated lipid nanoparticles with targeting vector have a higher percentage of cytotoxicity. The above findings were similar to A54-9 cells, but when compared to MCF-7 cells, the optimized formulation demonstrated a higher rate of inhibition due to folate overexpression on the cancer cells. The uptake mechanism may enhance and escalate the cytotoxic activity.

It was found that iron oxide nanoparticles are easily taken up by cancer cells compared to normal cells due to an increase in the need for nutrients for the angiogenesis process, where the iron oxides are degraded into iron ions in the lysosomal pH of cancer cells, which might provoke interactions between nanoparticles and the immune system. This leads to an increase in the availability of gallic acid on cancer cells to promote apoptosis. The best part about using iron oxide in cancer therapy is that it gets degraded and metabolized by the body and therefore does not accumulate in the body.

Among gallic acid and gallic acid iron oxide nanoparticles, surface-functionalized PEGylated lipid NPs has a higher cytotoxicity effect. This might be due to the increased circulation time of nanoparticles as well as PEGylation, which has the ability to enhance the retention time of the therapeutics on cancer cells. This could be attributed to preventing the opsonization process because PEGylation induces steric hindrance and can prevent immune recognition. In addition, the presence of a negative carboxyl group increases the surface charge of nanoparticles and enhances their uptake. However, (Hea-Young Cho 2015; Kumar Ganesan et al. 2021) reported that the surface targeting vector (Folate) may precisely target the drug on cancer cells, despite the fact that it retains its ability to bind to receptors after drug conjugation and attaches to the receptors located within caveolae (Mi et al. 2011), and it is internalized through the endocytosis pathway and

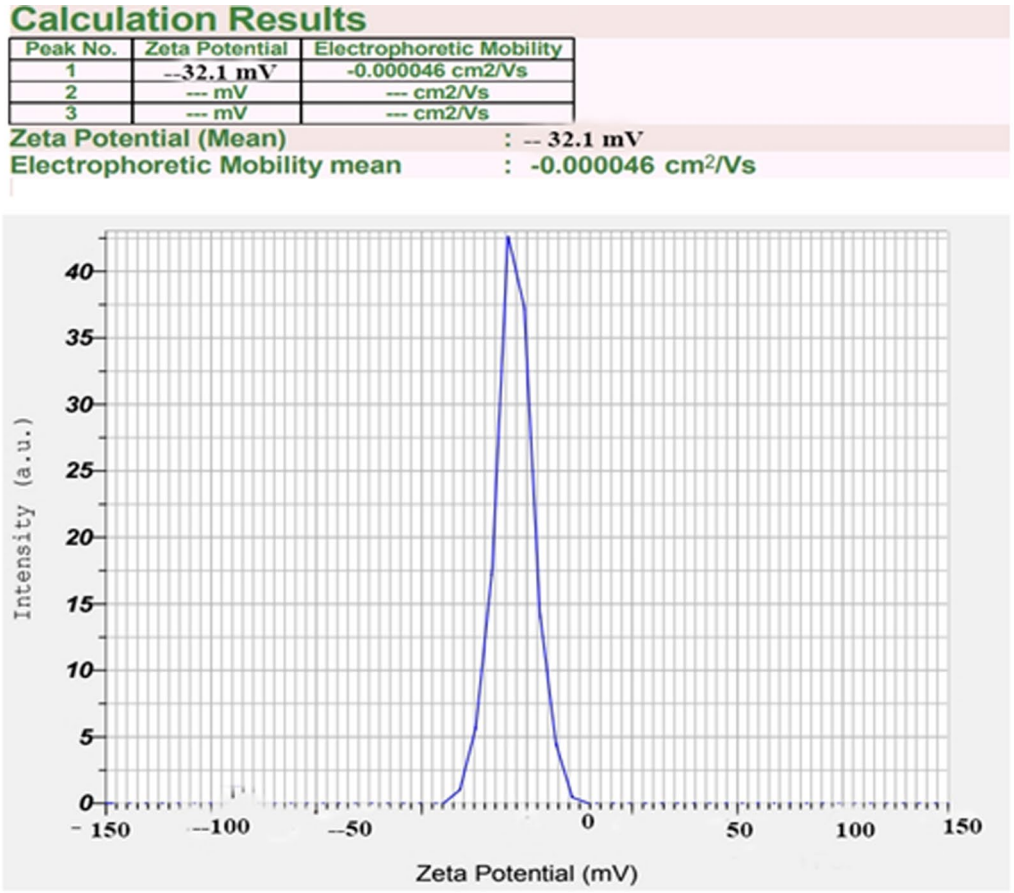

a) Zeta potential of optimized formulation

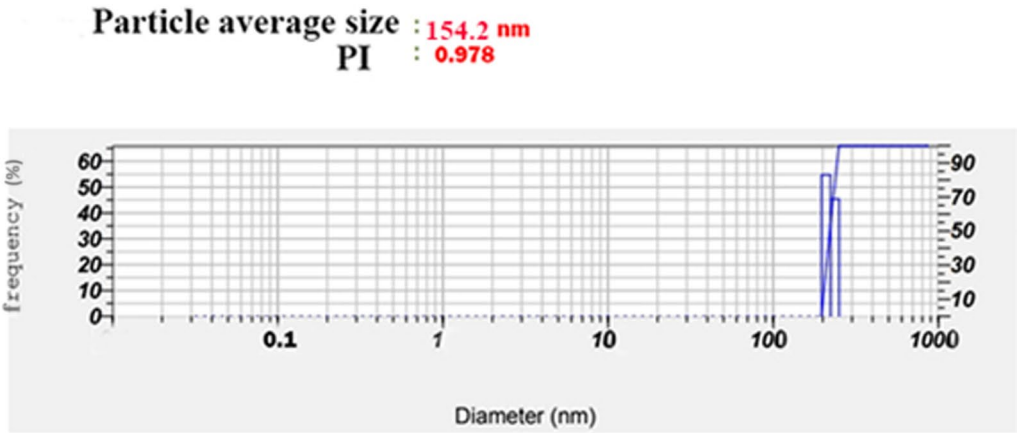

b) Particle size of optimized formulation

Fig. 9 **a** Zeta potential and **b** particle size of optimized formulation

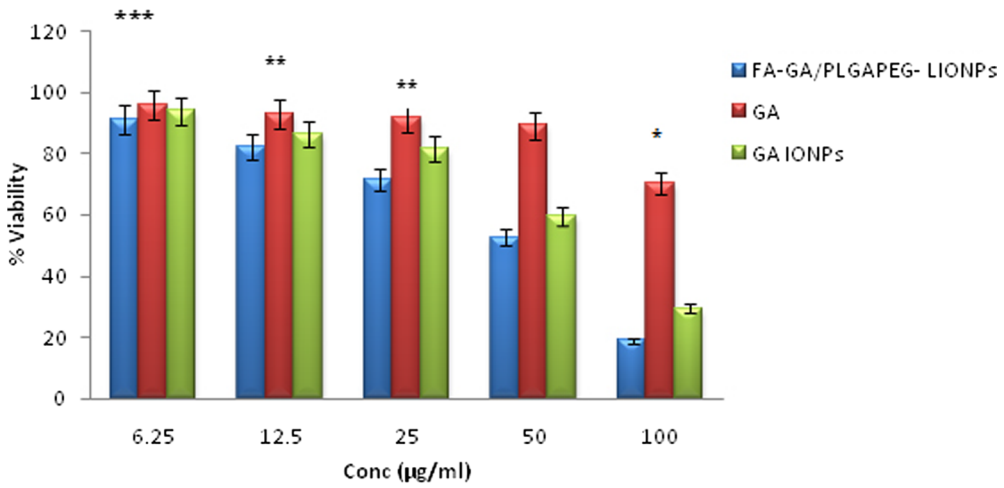

a) In-vitro cell line study (MCF-7) of the pure drug gallic acid (GA),Gallic acid iron oxide nanoparticles (GA IONPs), Folate tagged lipid nanoparticles (FA-GA/PLGA PEG-LIONPs) Data shown are means ± SD (n = 3, *p-value < 0.05, ***p-value < 0.001,p-<0.01 versus concentration.**

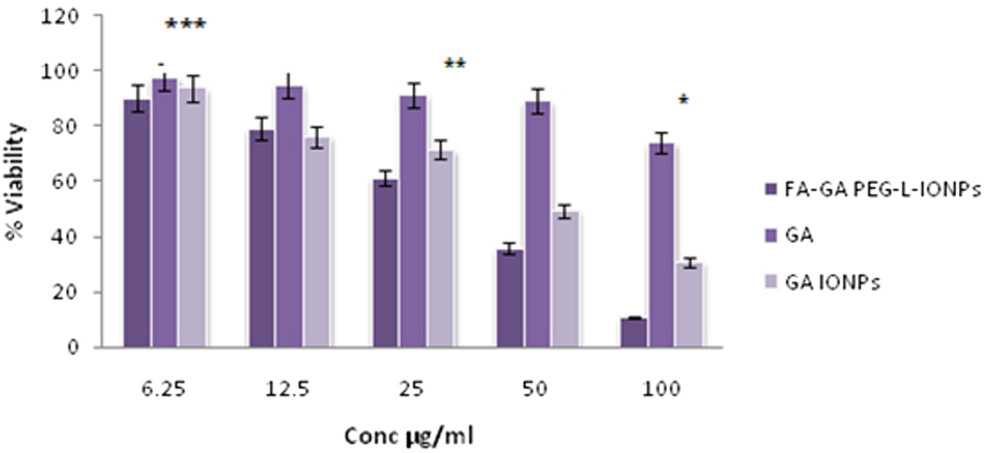

b) In-vitro cell line study (A54-9) of the pure drug gallic acid (GA),Gallic acid iron oxide nanoparticles (GA IONPs), Folate tagged lipid nanoparticles (FA-GA/PLGA PEG-

Fig. 10 **a** In vitro cell line study (MCF-7) of the pure drug gallic acid (GA), gallic acid iron oxide nanoparticles (GA IONPs), folate-tagged lipid nanoparticles (FA-GA/PLGA PEG-LIONPs). Data shown are means ± SD (n = 3, *P-value < 0.05, ***P-value < 0.001,**P < 0.01 versus concentration. **b** In vitro cell line study (A54-9) of the pure drug gallic acid (GA), gallic acid iron oxide nanoparticles (GA IONPs), folate-tagged lipid nanoparticles (FA-GA/PLGA PEG-LIONPs). Data shown are represented as means ± SD (*n* = 3, *P-value < 0.05, ***P-value < 0.001,**P- < 0.01 versus concentration

increases the availability of the drug in the cancer cells, which leads to a decrease in cell viability.

Cellular internalization study/Fluorescent staining for nuclear morphology study

Fluorescent microscopy images established the internalization of folate-conjugated gallic acid-loaded PEGylated lipid nanoparticles into MCF-7 cells. The cells that misplaced membrane reliability showed red staining throughout the nucleus. GANP also increased the number of annexin V staining cells in MCF-7 cells in a dose-dependent manner, as shown in Fig. 11. Gallic acid released from the nanoparticles may induce apoptotic cell death in MCF-7 cells, as evidenced by staining cells. The MCF-7 cells showed higher nuclei (blue) than MCF-7 cells, and the cells treated with GA NPs had red

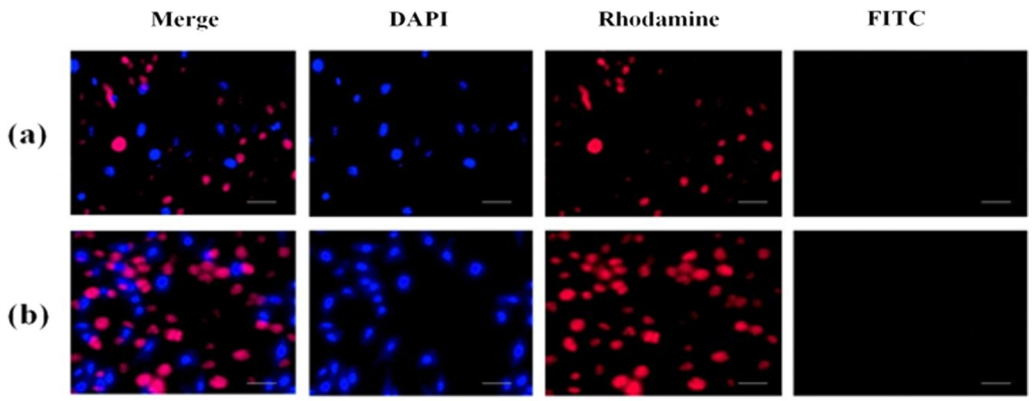

Fig. 11 Cellular uptake study (confocal microscopic images) of optimized formulation **a** 5 µg/ml concentration of gallic acid nanoparticles, **b** 20 µg/ml concentration of gallic acid nanoparticles

Table 2 The design and response of gallic acid-loaded nanoparticles according to the Box–Behnken experimental design

Run	*A*: X_1 lipid concentration	*B*:X_2 Polymer concentration	*C*:X_3 Drug concentration	Y_1 (Particle size)	Y_2 (Entrapment efficiency)	Y_3 (Drug release)
1	4	1	20	295.4 ± 1.2	29.2 ± 3.6	40.8 ± 2.1
2	4	0.5	20	295.2 ± 3.6	28.4 ± 4.2	42.8 ± 4.1
3	4	1.5	20	225.4 ± 7.2	58.1 ± 5.1	55.6 ± 6.2
4	4	0.75	20	154.4 ± 4.11	75.4 ± 2.1	90.4 ± 4.1
5	2	1	20	195.3 ± 4.4	68.91 ± 3.5	83.4 ± 4.4
6	2	1	20	265.4 ± 5.2	50.2 ± 4.1	42.8 ± 4.6
7	3	1	20	195.5 ± 5.3	68.91 ± 2.5	84.8 ± 6.1
8	1	1	20	195.1 ± 7.2	68.94 ± 2.9	82.9 ± 6.9
9	4	1	20	225.3 ± 1.5	58.5 ± 3.5	63.4 ± 7.2
10	4	1	20	195.2 ± 6.9	68.93 ± 5.2	84.4 ± 6.4
11	4	1	20	185.4 ± 4.3	46.2 ± 4.6	49.4 ± 7.1
12	4	1	20	190.6 ± 4.2	53.4 ± 4.1	60.5 ± 4.3
13	4	1	5	194.7 ± 6.1	40.6 ± 6.2	40.8 ± 5.1
14	4	1	10	160.7 ± 5.2	73.6 ± 5.1	84.6 ± 5.2
15	4	1	15	260.8 ± 2.6	40.3 ± 5.3	55.9 ± 7.1
16	4	1	20	189.5 ± 2.9	66.7 ± 5.6	82.8 ± 6.4
17	4	1	25	260.1 ± 3.1	42.8 ± 6.2	58.2 ± 7.5

Table 3 ANOVA for the quadratic model developed for the optimization of gallic acid lipid nanoparticles

Source	Sum of square	Df	Mean square	*F* value	*P* value
Model	4348.21	9	483.13	4.98	< 0.0001
Residual	679.70	7	97.10	–	
Lack of fit	67	3	225.66	2.76	0.0530
Pure error	2.73	4	0.68	–	
Corr. total	5027.9	16	–	–-	

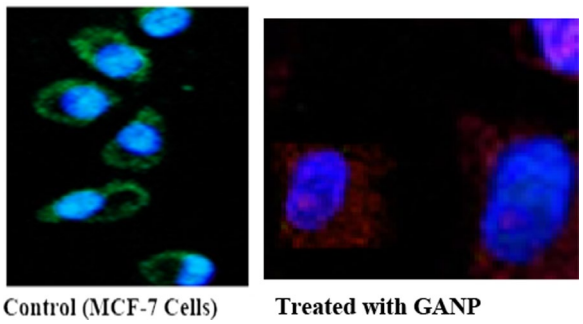

Fig. 12 Fluorescence microscopic images of GANPs (vs) control cells

Table 4 Similarity between experimental value and observed value

X_1	X_2	X_3	EXPERIMENTAL VALUE Y_1 76.8	Y_2 157.8	Y_3 91.3
0.952	0.903	0.725	Observed value (Y_1) 75.4	Y_2 154.4	Y_3 90.4

staining due to the presence of iron oxide (PS). The cells treated with GANP (merge) showed a higher level of subcellular localization (Khorsandi et al. 2020, Suraj 2020). These findings propose that the targeting similarity of the ligands in relation to PS drug conjugates identified for MCF-7 cells was functional and so enhanced the subcellular localization (Ramona-Daniela Pavaloiu et al. 2021) and attentiveness uptake within these cells.

DAPI staining was assessed to distinguish the potential nuclear changes like DNA damage, which are accountable for the cellular inhibitory effect of FA-GA/PLGA-PEGylated LIONPs related to the induction of cell apoptosis. Figure 12 represents the morphology of DAPI-stained nanoparticles treated with or without MCF-7 cell lines (control). In control, the green point represents the cytosol and the blue point represents the nuclei. Respectively, the cells treated with nanoparticles exhibited typical apoptotic morphology with cell shrinkage, nuclear fragmentation, and DNA condensation (Suraj 2020). Using DAPI staining, the whole nuclear morphology in the negative organized collection of cells was experimental.

Conclusions

The gallic acid-loaded PEGylated/lipid nanoparticles were formulated and optimized using the Box–Behnken model. FTIR, XRD, and DSC studies revealed that drugs and polymers do not interact. SEM and TEM results showed the prepared nanoparticles were spherical and round in shape with a lipid coating (bilayer). The zeta potential and particle size results were found to possess a negative value for nanoparticles; this indicates the stability properties of nanoparticles. The results of release studies indicate that gallic acid-loaded PEGylated nanoparticles offer a biphasic release. Cellular uptake studies and fluorescence imaging studies revealed that surface-functionalized GANPs have higher uptake and cytotoxicity activity. Overall, these findings shed light on the importance of PEGylation and lipid as well as the targeting moiety, which can change the release properties and increase the circulation time of the drug in the blood to precisely target breast cancer via clathrin-mediated endocytosis. In this process, particular ligands in an extracellular fluid bind to the receptors on the surface of the cell membrane (CM), forming a ligand–receptor complex. This ligand–receptor complex moves to a specialized region of the CM where they are invaginated through the configuration of clathrin-coated vesicles. Once inside the cell, clathrin coatings on the peripheral of the vesicles are excluded prior to fusion with early endosomes. The cargo within early endosomes will ultimately reach lysosomes via the endo-lysosomal pathway.

Abbreviations

GA: Gallic acid; IO: Iron oxide; GANP: Gallic acid nanoparticle; MTT: (3-(4,5-dimethylthiazol-2-yl)-2,5-diphenyltetrazolium bromide); DSC: Differential scanning calorimetry; FTIR: Fourier-transform infrared spectroscopy; TGA : Thermogravimetric analysis; XRD: X-ray diffraction; SEM: Scanning electron microscopy; TEM: Transmission electron microscopy; PLGA: Polylactic glycolic acid; FA: Folic acid; MCF-7: Human breast adenocarcinoma cell line; DSPE: Distearoyl-phosphoethanolamine; NPs: Nanoparticles; PLGA NPs: Polylactic glycolic acid nanoparticle; PEG: Polyethylene glycol; IONP: Iron oxide nanoparticles; DAPI: 4,6-diamidino-2-phenylindoles; OD: Optical density value; KBR: Potassium bromide; MPS: Mononuclear phagocyte system; VSM: Vibrating sample magnetometer; DMSO: Dimethyl sulfoxide; FITC: Fluorescein isothiocyanate; LIONPs: Lipid iron oxide nanoparticles.

Acknowledgements

The authors are grateful to the management, for the facilities. This publication is a part of PhD Thesis of The Tamilnadu Dr. M.G.R. Medical University, Chennai, Tamilnadu, India

Author contributions

UU contributed to design of the work by stepwise manner by providing an eminent idea for the content needed to write this manuscript, and SV carried out the study and analysed the report to writing the manuscript. All authors read and approved the final manuscript.

Funding

No funding was obtained for this study.

Availability of data and materials

All data and materials are available upon carried out by authors.

Declarations

Ethical approval and consent to participate

Not applicable.

Consent for publication

Not applicable.

Competing interests

No conflict of interest from authors.

Received: 14 June 2022 Accepted: 6 July 2022
Published online: 17 August 2022

References

Agabeigi R (2020) Novel chemo-photothermal therapy in breast cancer using methotrexate-loaded folic acid conjugated Au@SiO(2) nanoparticles. Nanoscale Res Lett 15:62. https://doi.org/10.1186/s11671-020-3295-

Arsianti A (2020) Synthesis, characterization, and cytotoxicity evaluation of gallic acid nanoparticles towards breast T47D cancer cells. Pharmacognosy J 12(2):321–327

Attallah OA, Shetta A, Elshishiny F (2020) Essential oil loaded pectin/chitosan nanoparticles preparation and optimization via Box–Behnken design against MCF-7 breast cancer cell lines. RSC Adv 10:8703–8708

Baiti RN, Ardhyananta H, KiratK El (2015) Effect of acidic and basic environment to the degradation behavior of PLGA nanocapsules for biomedical application. AMR 6:1123–1213
Baskararaj S, Panneerselvam T (2020) Formulation and characterization of folate receptor-targeted PEGylated liposome encapsulating bioactive compounds from *Kappaphycus alvarezii* for cancer therapy. Biotech 10(3):136
Bhanumathi R (2018) Drug-carrying capacity and anticancer effect of the folic acid- and berberine-loaded silver Nanomaterial to regulate the AKT-ERK pathway in breast cancer. ACS Omega 3(7):8317–8328
Brandenberger C, Mühlfeld C (2010) Quantitative evaluation of cellular uptake and trafficking of plain and polyethylene glycol-coated gold nanoparticles. Small 6(15):1669–1678
Chithrani BD, Ghazani AA, Chan WC (2006) Determining the size and shape dependence of gold nanoparticle uptake into mammalian cells. Nano Lett 6(4):662–668
Cho H-Y (2015) Preparation and evaluation of PEGylated and folate-PEGylated liposomes containing paclitaxel for lymphatic delivery. J Nanomat. https://doi.org/10.1155/2015/471283
Correcher R (2021) Role of gallic acid in the synthesis of carbon-encapsulated iron nanoparticles by hydrothermal carbonization: selecting iron oxide composition. ACS Omega 6:44.29547-29554
Dausend J, Musyanovych A, Dass M, Walther P (2008) Uptake mechanism of oppositely charged fluorescent nanoparticles in HeLa cells. Macromol Biosci 8(12):1135–1143
Dorniani D (2012) Preparation of Fe_3O_4 magnetic nanoparticles coated with gallic acid for drug delivery. Int J Nanomed 7:5745–5756
Dorniani D, Kura AU (2014) Vitro sustained release study of gallic acid coated with magnetite-PEG and magnetite-PVA for drug delivery system. Sci World J. https://doi.org/10.1155/2014/416354
Dorniani D, Saifullah B, Barahuie F (2016) Graphene oxide-gallic acid nanodelivery system for cancer therapy. Nanoscale Res Lett 11:491. https://doi.org/10.1186/s11671-016-1712-2
Ebadi M (2021) Drug delivery system based on magnetic iron oxide nanoparticles coated with (polyvinyl alcohol-zinc/aluminium-layered double hydroxide-sorafenib). Alex Eng J 60(1):733–747
Farran B (2020) Folate-conjugated nanovehicles: strategies for cancer therapy. Mater Sci Eng C Mater Biol Appl 107:110341. https://doi.org/10.1016/j.msec.2019.110341
Ganesan K (2021) Targeting engineered nanoparticles for breast cancer therapy. Pharmaceutics 13(11):1829
Guo W, Quan P, Fang L, DongmeiCun MY (2015) Sustained release donepezil loaded PLGA microspheres for injection: preparation, in vitro and in vivo study. Asian J Pharma Sci 10(5):405–414. https://doi.org/10.1016/j.ajps.2015.06.001
Hassani A, Mahdi M (2020) Preparation, characterization and therapeutic properties of gum arabic-stabilized gallic acid nanoparticles. Sci Rep 10:17808
Hassani A, Azarian MMS, Ibrahim WN (2020) Preparation, characterization and therapeutic properties of gum arabic-stabilized gallic acid nanoparticles. Sci Rep 10:17808. https://doi.org/10.1038/s41598-020-71175-8
Hu X, Ning P, Zhang R (2016) Anticancer effect of folic acid modified tumor-targeting quercetin lipid nanoparticle. Int J ClinExp Med 9(9):17195–17202
Ibrahim S (2021) Optimization for biogenic microbial synthesis of silver nanoparticles through response surface methodology, characterization, their antimicrobial, antioxidant, and catalytic potential. Sci Rep 11:770
KeWang (2014) Investigation of gallic acid induced anticancer effect in human breast carcinoma MCF-7 Cells. J Biochem Mol Toxicol. https://doi.org/10.1002/jbt.21575
Khan B (2021) In vitro sustained release of gallic acid from the size-controlled PEGylated magnetite nanoparticles. Chem Pap 75:5339–5352. https://doi.org/10.1007/s11696-021-01724-6
Khorsandi K, Kianmehr Z, Hosseinmardi Z, Hosseinzadeh R (2020) Anti-cancer effect of gallic acid in presence of low level laser irradiation: ROS production and induction of apoptosis and ferroptosis. Cancer Cell Int 13:20–32. https://doi.org/10.1186/s12935-020-1100
Makadia HK (2011) Poly lactic-*co*-glycolic acid (PLGA) as biodegradable controlled drug delivery carrier. Polymers 3(3):1377–1397
Mi Y, Liu Y, Feng SS (2011) Formulation of docetaxel by folic acid-conjugated d-alpha-tocopheryl polyethylene glycol succinate 2000 (Vitamin E TPGS(2k)) micelles for targeted and synergistic chemotherapy. Biomaterials 16:4058–4066
Niaz S (2022) Exploiting endocytosisfor non- spherical nanoparticles cellular uptake. Nanomanufacturing 2:1–6
Nicosia A (2021) Silver nanoparticles decorated with PEGylated porphyrins as potential theranostic and sensing agents. Materials 14:2764. https://doi.org/10.3390/ma14112764
Norton N, Youssef B (2020) Folate receptor alpha expression associates with improved disease-free survival in triple negative breast cancer patients. NPJ Breast Cancer. https://doi.org/10.1038/s41523-020-0147-1
Panariti A, Miserocchi G, Rivolta I (2012) The effect of nanoparticle uptake on cellular behavior: disrupting or enabling functions. Nanotechnol Sci Appl 5:87
Pavaloiu R-D (2021) Intracellular uptake study of polymeric nanoparticles loaded with cardiovascular drugs using confocal laser scanning microscopy. Chem Proc 3:140. https://doi.org/10.3390/ecsoc-24-08427
Priyadarshani S (2021) Optimally biosynthesized, PEGylated gold nanoparticles functionalized with quercetin and camptothecin enhance potential anti-inflammatory, anti-cancer and anti-angiogenic activities. J Nanobiotech 19:84
Radwan SAA, El-Maadawy WH, Yousry C, ElMeshad AN, Shoukri RA (2020) Zein/phospholipid composite nanoparticles for successful delivery of gallic acid into aHSCs: influence of size, surface charge, and vitamin A coupling. Int J Nanomed 15:7995–8018. https://doi.org/10.2147/IJN.S270242
Rashidi L (2014) A cellular uptake and cytotoxicity properties study of gallic acid-loaded mesoporous silica nanoparticles on Caco-2 cells. J Nanoparticle Res. https://doi.org/10.1007/s11051-014-2285-6
Rathi V (2012) Folate- decorated PLGA nanoparticles as a rationally designed vehicle for the oral delivery of insulin. Nanomedicine 7(9):1311–1337
Rejman J, Oberle V, Zuhorn I, Hoekstra D (2004) Size-dependent internalization of particles via the pathways of clathrin-and caveolae-mediated endocytosis. Biochem J 377:159–169
Sartaj A (2021) Polymeric nanoparticles: exploring the current drug development and therapeutic insight of breast cancer treatment and recommendations. Polymers 13(24):4400
Shah ST, Yehyel WA, Saad O (2017) Surface functionalization of iron oxide nanoparticles with gallic acid as potential antioxidant and antimicrobial agent. Nanomaterials 7:306. https://doi.org/10.3390/nano7100306
Sharaf NS (2022) Applying Box–Behnken design for formulation and optimization of PLGA-coffee nanoparticles and detecting enhanced antioxidant and anticancer activities. Polymers 14:144. https://doi.org/10.3390/polym14010144
Sharma D, Maheshwari D (2014) Formulation and optimization of polymeric nanoparticles for intranasal delivery of lorazepam using box–behnken design: in vitro and in-vivo evaluation. Biomed Res Int 14:156010
Singh R, Kesharwani P (2020) Development and characterization of folate anchored Saquinavir entrapped PLGA nanoparticles for anti-tumor activity. Drug Dev Ind Pharm 41(11):1888–1901
Sinha P, Udhumansha U, Rathnam G, Ganesh M (2018) Capecitabine encapsulated chitosan succinate-sodium alginate macromolecular complex beads for colon cancer targeted delivery: in vitro evaluation. Int J Biol Macromol 117:840–850
Socoliuc V (2020) Magnetic nanoparticle systems for nanomedicine: a materials science perspective. Magnetochemistry 6(1):2. https://doi.org/10.3390/magnetochemistry601000
Soma D, Attari Z, Reddy MS, Damodaram A (2017) Solid lipid nanoparticles of irbesartan: preparation, characterization, optimization and pharmacokinetic studies. Braz J Pharm Sci 53(1):15012
Suk JS, Xu Q, Kim N, Hanes J, Ensign LM (2016) PEGylation as a strategy for improving nanoparticle-based drug and gene delivery. Adv Drug Deliv Rev 99:28–51. https://doi.org/10.1016/j.addr.2015.09.012
Ubaidulla U, Ahmad FJ, Khar RK, Tripathi P (2008) Optimization of chitosan succinate and chitosan phthalate microspheres for oral delivery of insulin using response surface methodology. Pharm Dev Technol 26:1–10. https://doi.org/10.1080/10837450802409461

Wan FatihahKhairunisa Wan Nor (2018) Synthesis and physicochemical properties of magnetite nanoparticles (Fe_3O4) as potential solid support for homogeneous catalysts, Malaysian J Anal Sci 22(5):768–774, https://doi.org/10.17576/mjas-2018-2205-04
Yang C, Merlin D (2020) Lipid-based drug delivery nanoplatforms for colorectal cancer therapy. Nanomaterials 10:1424. https://doi.org/10.3390/nano10071424
Yetisgin AA (2020) Therapeutic nanoparticles and their targeted delivery applications. Molecules 25:2193

Publisher's Note